XVI International Conference on Computational Plasticity. Fundamentals and Applications
COMPLAS 2021
E. Oñate, D. Peric, M. Chiumenti and Eduardo de Souza Neto (Eds)

INFLUENCE OF TOPOLOGY HYBRIDIZATION AND FUNCTIONAL GRADING ON COMPRESSIVE PROPERTIES OF SHEET-BASED TPMS LATTICE CORES

Chukwugozie J. Ejeh[a,b], Imad Barsoum[a,b,*] and Rashid K. Abu Al − Rub[a,b]

a. Advanced Digital & Additive Manufacturing Center, Khalifa University of Science and Technology, 127788, Abu Dhabi, United Arab Emirates.

b. Department of Mechanical Engineering, School of Engineering, Khalifa University of Science and Technology, 127788, Abu Dhabi, United Arab Emirates.

* Email: imad.barsoum@ku.ac.ae, web page: https://www.ku.ac.ae/

Keywords: Hybridization, Functional grading, triply periodic minimal surfaces, Specific energy absorption.

Abstract: Lattice cores are essential for achieving high strength, and lightweight design of additive manufactured engineering components. The influence of topology hybridization and functional grading (i.e., cell size and relative density gradation) on the quasi-static compressive properties of the mathematically-derived sheet-triply periodic minimal surfaces (TPMS)-based lattice structures are numerically investigated in this paper. The objective is to propose an advanced meta-material design for improved mechanical functionality. The popularly investigated Schwartz diamond (D), F-Rhombic dodecahedron (FRD), and Schoen gyroid (G)topologies are considered. TheJohnson-Cook plasticity model based on an additive manufactured AlSi10Mg tensile test specimen is employed for the finite element simulations.Numerical results such as elastic modulus, yield strength, ultimate strength, specific energy absorption,and energy absorption efficiency of the lattices serve as the means of comparison. Based on the findings, a paradigm shift in the failure behavior was noticed with the functionally graded lattices, e.g. from shear-dominated to layer-by-layer collapse. The latter is desirable in the sense that, more kinetic energy can be consumed during failure. Among the studied single TPMS morphologies, the FRD lattice showed to exhibit superior compressive properties in all three design categories. Unlike the shear-band failure observed with the uniform G and D lattices, the FRD topology demonstrated a multi-segment cell layer collapse without functional gradation. On the contrary, the hybrid structures demonstrated an entirely different failure trend. Failure began in the topology with relatively the highest surface-area-to-volume ratio. Furthermore, an increase in strength was observed when the topology at the transition region began to deform plastically. Also, the novel topology (Multi-E1) showed unprecedented failure behavior with minimal stress concentrations coupled with considerably high mechanical performance. Overall, the relative density graded FRD lattice performed best mechanically.Hence, higher compressive properties of cellular materials can be achieved with the relative density graded FRD micro-architecture.

1. INTRODUCTION

Nature-inspired,lightweightporous materials with complex sub-unit cellular configurations, are perceived to revolutionize the field of meta-material design. High precision and relatively low-cost fabrication of these porous materials are possible with recent advancements in additive manufacturing processes. The mechanical properties of cellular materials such as stiffness, energy absorption, and strength, are directly related to theirtopological features (i.e., cell size, cell morphology, inter-cellular connectivity of the cells,surface-area-to-volume ratio, porosity, etc.) [1]. Literature shows that the mechanical performance of cellular materials can be tailored to meet the desired functionality. This is possible through a controlled modification in their geometric properties [2]. However, it is rather challenging to arrive at a scheme specifically for the engineering need, capable of appropriately attenuating the lattice geometric features [1].

In recent times, material science researchers have directed their focus to study the mechanical functionality of lattice structures. Among the family of periodic cellular structures, the mathematically-obtained triply periodic minimal surface (TPMS)-based lattices are the most preferred. More importantly, the sheet-based ones portray desirable failure behavior with a reduced possibility of stress concentrations mainly due to their minimal surface-like topology. Here, failure is governed by the wrinkling of the sheet-winkling because of shear stresses. On the contrary, failure in strut-based lattices begins at the strut's junctions and shear-dominated in the sense that early buckling of the struts is noticeable upon compression loading [3].

Functionally graded sheet-based TPMS lattice structures (i.e., diamond and Schoen gyroid) are reported to predominantly fail by a layer-to-layer fashionupon uniaxial compression loading[4]. Conversely, the topologies with uniform properties assume a shear-band failure along the lattice planes of symmetry (45° and 90° plane) during similar loading conditions [5]. Because of the controlled failure behavior of the lattice core, the additive manufactured graded samples attained higher compressive strength and energy absorption. A similar conclusion was arrived at by Montazerian et al. [6] when studying the compressive properties of the Schwartz primitive, Schoen gyroid, and diamond porous scaffolds. Furthermore, the polymetric cellular structures (i.e.,the I-wrapped package and primitive lattices) whose relative density was graded perpendicularly to the loading direction were reported to perform poorly as opposed to those graded in-line with the loading axis[7]. Also, Alketan et al. [4] in their work found that cell size gradation of the lattice structure could as well improve the mechanical properties and that topology hybridization of two or more lattices could be promising mechanically.

The sigmoidal function was employed by Alketan et al. [4] tomodel the smooth transition between the diamond and gyroid topology to form the hybrid lattice structures. Up on quasi-static compression loading on the additively manufactured lattices, an enhancement of the mechanical properties was noticed [4]. The structures loaded parallel to the direction of hybridization yielded the best performance (see Alketan and Abu Alrub [1] for a comprehensive review).

In this paper, the compressive properties of functionally graded and advanced hybrid lattice structures are investigated through finite element (FE) analysis. Adding to previous works in the literature, we propose a new sheet-TPMS-based topology with the potential of performing better mechanically upon axial loading than those reported. Details on the design strategies are discussed.

2. MATERIALS AND METHODS

2.1 Design Methodology

The level-set approximation relationship $\varphi_s$is popularly used to formulate the TPMS-based cells. The relationship is specific for each type of TPMS cell. Corresponding level-set approximation equation for the Scheon gyroid (G), Schwartz diamond (D) and Schoen F-Rhombic dodecahedron (FRD) cells are as shown in Eqns. (1)-(3), respectively, where c is the level-set constant. Note that, a TPMS is formed when $c = 0$. Here, $\omega_x = 2\pi\alpha/L_x$, $\omega_y = 2\pi\beta/L_y$ and $\omega_z = 2\pi\gamma/L_z$ denote the spatial periodicity of the iso-surface embedded in $\mathbb{R}^3$ space, where L is an arbitrary constant that controls the size of the cell. Note that, $L_x = L_y = L_z$ and $\alpha = \beta = \gamma$ must hold to generate uniformly spawned representative minimal surface, such that,α, β and γ jurisdict the repeatability of the cells in the$x$, y and$z$ axes. For$\alpha = \beta = \gamma = 3$, a cell-matrix of $3 \times 3 \times 3$ (27 cells) is formed, as used in this paper.

$$\varphi_G \equiv \cos(\omega_x x)\sin(\omega_y y) + \cos(\omega_y y)\sin(\omega_z z) + \cos(\omega_z z)\sin(\omega_x x) \quad (1)$$

$$\varphi_D \equiv \cos(\omega_x x)\cos(\omega_y y)\cos(\omega_z z) - \sin(\omega_x x)\sin(\omega_y y)\sin(\omega_z z) = c \quad (2)$$

$$\varphi_{FRD} \equiv 4(\cos(\omega_x x)\cos(\omega_y y)\cos(\omega_z z)) - (\cos(2\omega_x x)\cos(2\omega_y y) + \cos(2\omega_y y)\cos(2\omega_z z) + \cos(2\omega_x x)\cos(2\omega_z z)) = c \quad (3)$$

In the MATLAB code, a sheet-TPMS,φ_{sh} is formed by implementing the relation $\varphi_{sh} = -1 * (\varphi_s^2 - t^2)$. Herein, $t$controls the sheet's thickness. The higher the value of$t$, the more chunky the sheet becomes [1, 4].

2.1.1 Relative Density Gradation

The relative density (ρ_r) of TPMS-based lattices is graded by numerically implementing the linear function; $\rho_r = \text{slope} * t + \text{intercept}$. It relates the volume fraction ρ_r and the constantt. The rule for gradation indicates that, when$y = 0$, $t = t_0$ (corresponding t value for ρ_{r_0}), andat $y = 1$ (assuming a unit cube), $t = t_1$ (corresponding t value for ρ_{r_1}). Hence, $t = t_0 + y * (t_1 - t_0)$.In this work, the lattice is graded from 16 – 10 % relative density in the direction of loadingas shown in Fig. 1. Modeledt values for the G, D, and FRD lattices at 16 % and 10 % relative densities are as follows; $c_0 = 0.249$ and $c_1 = 0.158$, $c_0 = 0.136$ and $c_1 = 0.089$, and $c_0 = 0.376$ and $c_1 = 0.239$, respectively. Note that, RD stands for cell size graded in the geometry nomenclature.

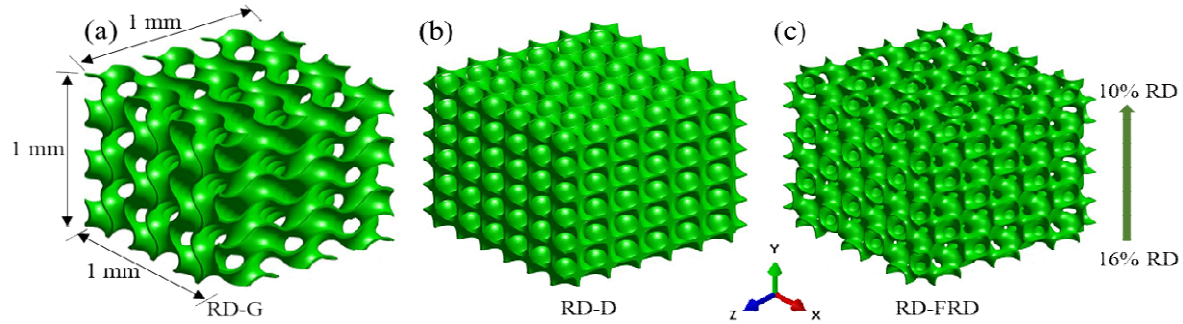

Figure 1: Relative density graded; (a) gyroid lattice, (b) diamond lattice, and (c) F-Rhombic Dodecahedron lattice.

2.1.2 Cell Size Gradation

Here, the cell size of the lattice is graded in the y-direction by expressing the spatial periodicity terms ωas a function of $y$as shown in Eq. (4), given that, $L_x = L_y = L_z = 1$, where a and b are arbitrary constants derived from solving the complete differential equations [4]. The solution to the differential equation reveals that;$a = -y_{min} * k + 1$ and $= 0.5 * (y_{min})^2 * k$, where $k = (m-1)/(y_{max} - y_{min})$, if $y_{min} \leq y \leq y_{max}$, and $m$is the cell size multiplier[4]. Hence, we use a cell size multiplier, $m = 1.5$ to construct3 cells at $y = y_{min}$, and 4.5 cells at $y = y_{max}$, as seen in Fig. 2.A cell size multiplier of 1.5 is used based on previous studies by Alketan et al. [3], where the effect of compaction is felt near the loading surface. Note that, CS stands for cell size gradation in the nomenclature.

$$\omega = \begin{cases} \omega_x = k * y + a \\ \omega_y = k * y + a \\ \omega_z = \left(\frac{k}{2}\right) * y + a + b/y \end{cases} \quad (4)$$

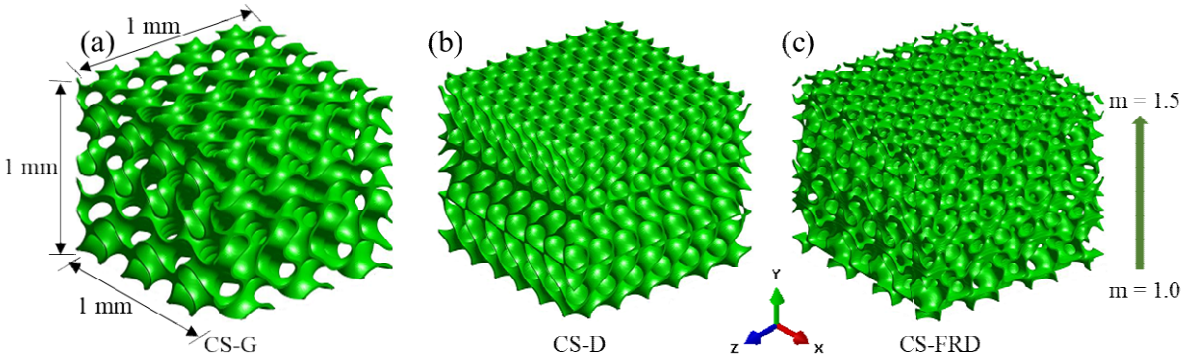

Figure2: Cell size graded; (a) gyroid lattice (CS-G), (b) diamond lattice (CS-D), and (c) F-Rhombic Dodecahedron lattice (CS-FRD).

2.1.3 Linear Topology Hybridization

The βfunction given in Eq. (5) presents aneffective way of modulating the smooth merging of two morphologies [8].The growth unfold at r= 0 and climax at $r = r_e$ such that$0 \leq r \leq r_e = 1$. The transitioning is symmetric at $r_m = 0.5$. It follows that, at $y = 0$, $\beta = 0$ and$\varphi_{hybr} = \varphi_{tpms1}$, and when $y = 1$, $\beta = 1$ and $\varphi_{hybrid} = \varphi_{tpms}$. Note that, $\varphi_{tpms1}$and φ_{tpms2} refers to

the level-set equation for the first and second TPMS-based topology to be hybridized. Therefore, the third phase is constructed at $\beta = 0.5$(50-50 % hybridization) when $y = r_m = 0.5$. Notwithstanding, the topologies are connected throughout the transition regime by the mathematical linear relationshippresented in Eq. (6).The modeled hybrid geometries comprising of the G and D lattices (Multi-1), FRD and Glattices (Multi-2), and the FRD and D lattices (Multi-3)can be viewed in Fig. 3.

$$\beta = \left(1 + \frac{r_e - r}{r_e - r_m}\right)\left(\frac{r}{r_e}\right)^{\frac{r_e}{r_e - r_m}} (5)$$

$$\varphi_{hybrid} = \varphi_{tpm} \quad (1 - \beta) + \beta\, \varphi_{tpm} \quad (6)$$

Herein, advanced topology hybridization schemes can be realized using the explicit function developed by Alketan and Abu AlRub [9]. As shown in Fig. 3(d) and (e), the Multi-4 geometry is built by assuming $y_j = -0.5$ for φ_G, $y_j = 0$ for φ_D, and $y_j = 0.5$ for φ_{FRD} for a box bounded between -0.5 and 0.5, while $x_i = 0$ and $z_k = 0$. Similarly, for the Multi-E1 case, $x_i = 0$, $y_j = 0$ and $z_k = 0$, where n, denote the number of cell types. Multi-E1 is atechnical name given to new lattice design developed through a controlled 3D merging of the FRD, D, and G cell types. Here, E stands for extended hybridization.

$$w_i(x, y, z) = \frac{1 + e^{\left(h\left(\|x - x_i\|^2 + \|y - y_j\|^2 + \|z - z_k\|^2\right)\right)}}{\sum_{i,j,k=1}^{n}\left[1 + e^{\left(h\left(\|x - x_i\|^2 + \|y - y_j\|^2 + \|z - z_k\|^2\right)\right)}\right]} (7)$$

$$\varphi_{multi-morpholog}\ (x) = \sum_{i=1}^{n} w_i(x)\, \varphi_i(x) (8)$$

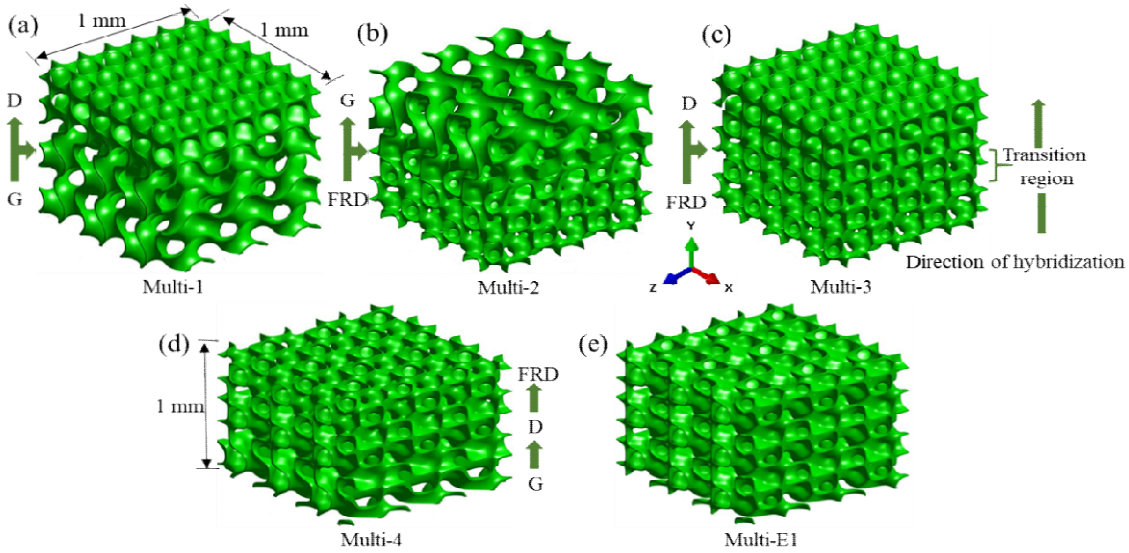

Figure 3: Linearly hybridized porous geometries; (a) G and D lattices, (b) FRD and G lattices, (c) FRD and D lattices, (d) G, D, and FRD lattices, and (e) 3D hybridization of the FRD, D and G lattices.

2.2 Constitutive Material Model and Properties

Elastic-plastic material behavior is modeled in this paper. Johnson-Cook (JC) plasticity model is employed to numerically describe the plastic response of the lattice cores. The mathematical model as shown in Eq. (9) relates the equivalent stress responsible for plastic deformation as a function of the material's yield strength, A coefficient of strain hardening,B, strain hardening exponent, n, and the equivalent plastic strain, ε_e^p [2].

Tensile stress-strain data of additively manufactured (in the horizontal direction) Aluminium alloy (AlSi10Mg) fabricated throughselective laser melting process is used to calibrate the JC plasticity model parameters as shown in Table 1 [10]. The JC plasticity model correlates well with experimental data as shown in Fig. 4.

$$\sigma = A + B(\varepsilon_e^p)^n (9)$$

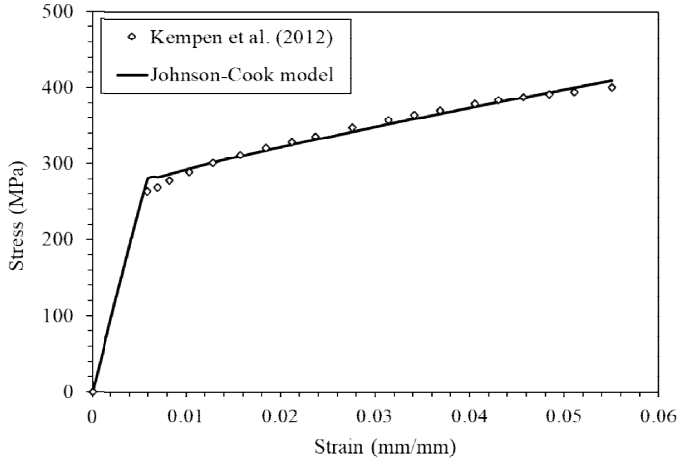

Figure4: Compares of the true tensile stress-strain curve, and curve-fitted JC plasticity model of AlSi10Mg [10].

Table 1: SLM AlSi10Mg properties and JC plasticity model parameters [10].

JC plasticity model parameters			Elastic properties		Mass properties
A [MPa]	B [MPa]	n	Young's modulus [MPa]	Poisson's ratio	Mass density [Tonne/mm^3]
250.63	1,560.62	0.79	69, 000	0.33	2.64×10^{-9}

2.3 Computational Procedure

The 10-node quadratic, tetrahedron (C3D10) meshing scheme with an element size of 0.01 mm is employed to discretize the lattices displayed in Figs. (1)- (3). The choice of seed size is based on a conducted mesh sensitivity study. To account for friction during surface-to-surface and surface-node interaction, the hard contact option in Abaqus™ is activated with a friction coefficient of 0.4 to mimic the physical surface roughness of printed samples. The compression plates are modeled as rigid bodies. Displacement-controlled compression loading is applied to the compression plates up to a strain level of 80 % to ensure that densification is reached. The FE codeAbaqus/Explicit Dynamics™ was utilized to simulate a low strain rate (quasi-static process).

2.4 Specific Energy Absorption Calculation

Specific energy absorption (SEA) is calculated analytically using the expression in Eq. (10). The sum of the product of the stress and change in the strain at every time step is divided by the relative density, $\rho_r$of the porous material. Most importantly, energy absorption efficiency, I, is defined as the ratio of the total energy absorbed by the lattice to that of an idealized condition where all the kinetic energy transmitted by the load is absorbed [11]. It is an effective way to compare the EA performance of lattice designs. The analytic model shown in Eq. (11) is used for computing, I, whereσ_d is the idealized maximum stress of the cushion made of rather AlSi10Mg [11].

$$SEA = \frac{1}{\rho_r}\int_0^{\varepsilon_d} \sigma d(\varepsilon) \quad (10)$$

$$I = \frac{\rho_r}{\sigma_d * \varepsilon_d}\, SEA \quad (11)$$

3. RESULTS AND DISCUSSION

3.1 Sampling and Geometric Error

Generally, the modeled and actual relative densities differ to an extent. The danger is, a large discrepancy may cause a wrong reflection of the actual compressive properties of the lattices. To address this issue, a correction factor $c_f$is developed to capture the geometric error for the predicted E, and the total E_a is divided by the actual relative density of the lattices as tabulated in Table1, to yield the SEA. The $c_f$is the ratio of the modeled relative density to actual relative density, such that the correct elastic modulus $E_a = E * c_f$.

Table 2: Design considerations and estimated geometric relative error.

Sample	Modeled $\boldsymbol{\rho_r}$ [%]	Actual $\boldsymbol{\rho_r}$ [%]	Relative Error [%]	$\boldsymbol{c_f}$
	Uniform property			
G	13.0	12.98	0.15	1.0015
D	13.0	12.74	2.00	1.0204
FRD	13.0	12.88	0.92	1.0093
	Relative density gradation			
RD-G	16 – 10.0	12.92	0.62	1.0062
RD-D	16 – 10.0	12.68	2.46	1.0252
RD-FRD	16 – 10.0	12.70	2.30	1.0236
	Cell size gradation			
CS-G	4 – 6 cells	12.84	1.23	1.0125
CS-D	4 – 6 cells	12.53	3.62	1.0375
CS-FRD	4 – 6 cells	12.24	5.85	1.0621
	Multi-morphology			
Multi-1 (G-D)	13.0	13.13	1.00	0.9901
Multi-2 (G-FRD)	13.0	13.03	0.23	0.9977
Multi-3 (FRD-D)	13.0	13.07	0.54	0.9946
Multi-4	13.0	13.50	3.84	0.9630

Multi-E1	13.0	13.57	4.38	0.9580

3.2 Qualitative FE Analysis

Generally, failure in lattice cores begins with the cell layer closest to the loading surface. From the equivalent Mises stress contours shown in Figs. (5)-(6), two common failure modes are usually observed such as shear-dominated failure and layer-wise subsidence of the cellular structures. The former is common with the uniform topologies, while the functionally graded ones exhibit the layer-by-layer collapse trend (see Fig. 5(f)). The latter is more desirable to avoid catastrophic damage while absorbing the energy during typical fatigue-crack propagation scenarios. Multi-sub layer subsidence is noticed with the FRD lattice irrespective of an alteration in its geometric properties. Insight from the FRD lattice topology shows centralized and transverse self-supporting properties with void spaces at the corners. The presence of the architectured voids at every sub-layer gives the structure better control over quick subsidence. Furthermore, 45° shear-band failure is noticed with the uniform D lattice as indicated in Fig.5(b). In physical application, fatigue failure would onset at that locus[12]. On contrary, minimal stress clustering at the transition region is realized in the hybrid geometries, especially with the Multi-E1 lattice design (see the color band for maximum Mises stress in Fig. 6(g) and compare with Fig. (5). This confirms the effectiveness of the β function to create smooth transitioning between the porous morphologies. Consequently, a reduced tendency for stress shielding effect in physical applications. However, major plastic slip lines are observed at the transition interface between the G and FRD lattice, as shown in Fig. 6(e). This could be due to gross dissimilarities in their shape and possibly strength.

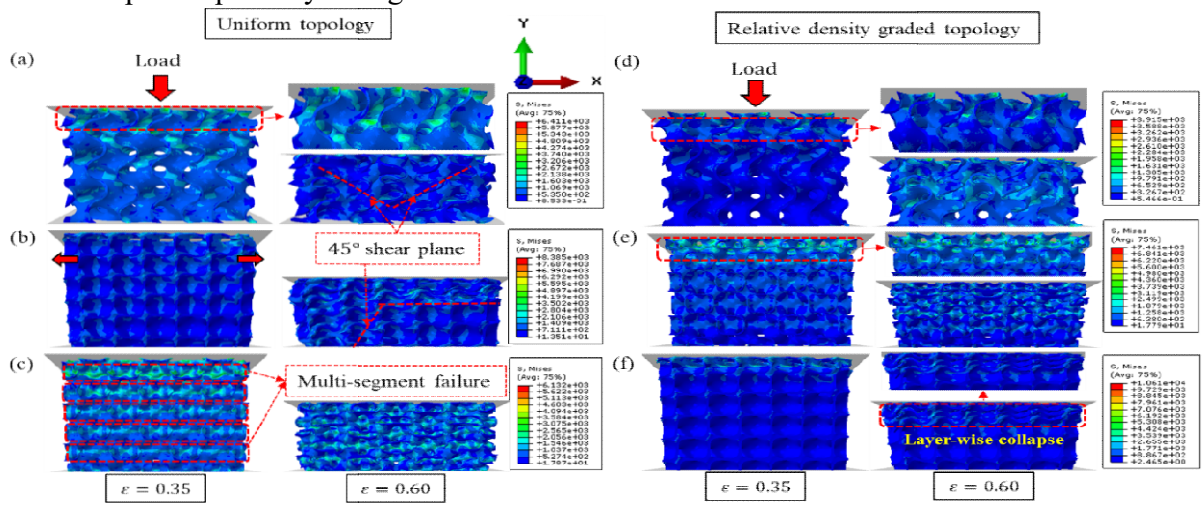

Figure 5 Mises stress contours at different strain levels for compression-loaded; (a) G lattice, (b) D lattice, and (c) FRD lattice. To the right; (d) RD-G lattice, (e) RD-FRD lattice, and (f) RD-D lattice.

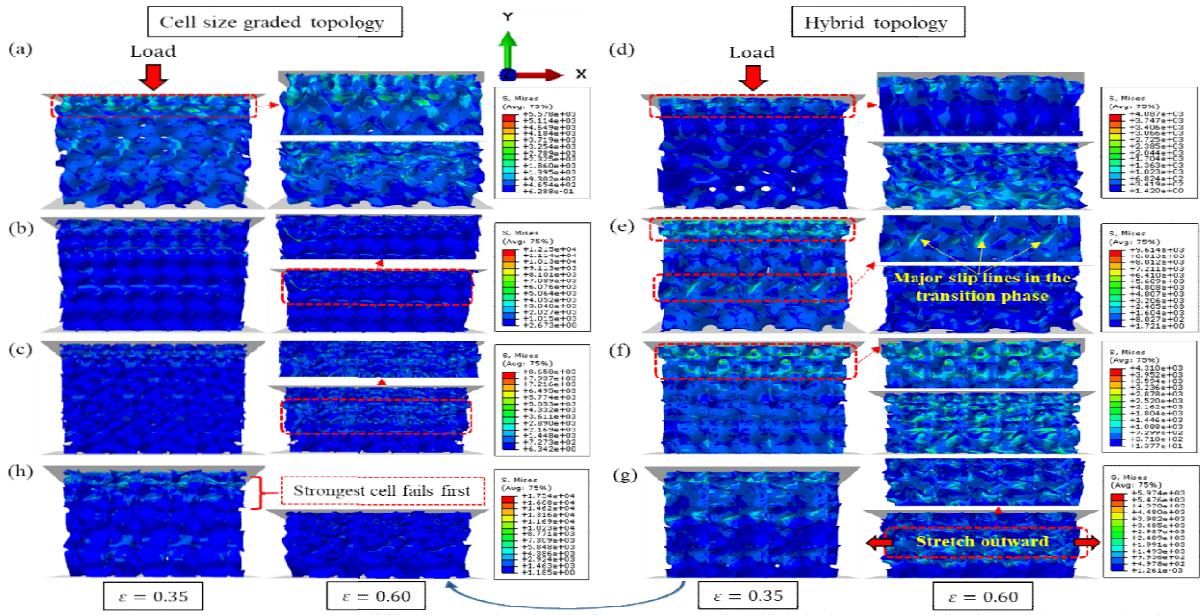

Figure 6: Mises stress contours at different strain levels for compression-loaded;(a) CS-G lattice, (b) CS-D lattice, and (c) CS-FRD lattice. To the right; (d) D-G lattice, (e) FRD-G lattice, (f) lattice, (g) Multi-E1 lattice, and (h)FRD-D-G lattice

3.3 Quantitative FE Analysis

The modulus of elasticity$E$for the lattices is evaluated from the linear portion of thestress-strain curves(see Fig. 7). Beyond the linear proportional limit, the onset of plastic deformation takes place in the response of the lattice material. The yielding strength, σ_Y is estimated at 0.2% offset strain, and the peak stress across the entire plastic regime is denoted σ_U. ForTPMS materials, multiple stress peaks and valleys are experienced owing to local plastic collapse and densification during compression. The total energy absorbed by the material in the process is equivalent to the area under the stress-strain graph up to the densification strain. A summary of the numerically derived elastic modulus, yield and ultimate strength, densification strain, and specific energy absorption is presented in Table 3. It is worth noting that, on final densification, a sharp rise in stress level would be noticed (see Figs. 7(a)-(d)). The point on the horizontal axis at which the tangent to that slope is interpreted as the densification strain ε_d. Estimation of *SEA* and *I* terminate at this strain level.

As discussed previously, variation in the topological properties of lattices would eventually cause a change in the failure behavior and their mechanical properties at large. With the relative density graded cellular structure, the layer of cells with relatively lower thickness would fail first (See Fig. 7(b) and Figs. 5(d)-(f)). Due to the smooth increase in relative thickness, a progressive collapse of the cell layers would occur, as highlighted in Fig. 5(f). The orderly failure of the cells contributed to the increase in *SEA* and *I*, as stipulated in Table 3. In the case of cell size gradation, we find that the cells at the top (close to the loading surface) are more compacted than those below. The larger the number of cells, the higher the strength of the lattice. However, this is not always the case, since at some point the strength of the lattice will cease from increasing. At this point, the effective material property of cellular material is determined. Given that compaction affects the mechanical properties of porous materials, an

increase in the overall stiffness of the lattice will be noticed as in the case of this work. On further collapse, the strength begins to decrease on account of the low compaction effect. Further to this, an increase in strength would be noticed just as described in Fig. 7(c). This comes as a result of densification taking place in the second cell layer, and so on. Comparatively, the functionally graded FRD architecture showed to achieve the best performance on compression loading. It is important to highlight that, a significant loss in strength was noticed with the CS-FRD lattice before the ε_d is reached. The large nature of the cell size compared to those at the upper layer could be the reason. A similar trend is spotted with the CS-G lattice. However, because of modeling difficulties, the CS-D lattice failed to densify. Hence, a red star is used in the plot to identify how far the simulation could reachas shown in Fig. 7(c). Notwithstanding, some important mechanical properties like stiffness and yield strength are determined. Strictly speaking, the FRD lattice at the initial stage of loading does not perform well mechanically. However, on further loading beyond $\varepsilon = 0.08$, it begins to gain strength at a very fast rate, thereby yielding superior compressive properties like $\sigma_U$and SEA as revealed in Table 3. Nevertheless, when the FRD lattice is hybridized with other topologies, the predicted mechanical properties may increase or decrease.

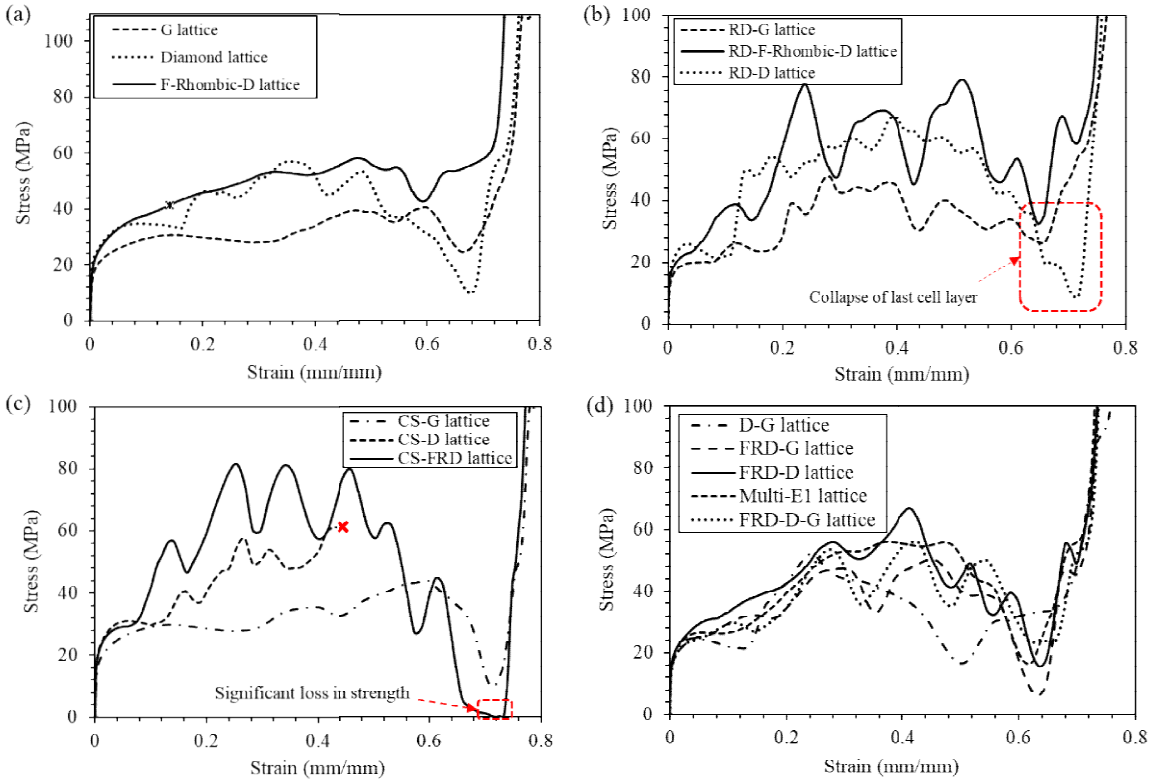

Figure 7: Compressive stress-strain curve for; (a) uniform lattices, (b) relative density graded lattices, (c) cell size graded lattices, and (d) hybrid cellular structures.

Studies on the compressive properties of the hybrid lattices revealed important insights on the influence of hybridization. The G lattice indicates improved mechanical behavior when hybridized with the D cell, and when graded in relative density. However, on account of their curvature with a high tendency of collapsing on compression, the G structure performed less

mechanically compared to the other cell types. The best performance of the D lattice is attained when hybridized with the FRD cell type. Reason being that, compared to the G lattice, the FRD cellular structure has the highest strength in axial loading. Therefore, hybridizing a relatively low mechanically performing cell type with an FRD structure would increase its performance. However, this is not the case with the FRD. Findings convey that the FRD lattice achieved better mechanical performance on functional grading alone.

Energy absorption efficiency, *I*, is another important basis for comparing the success of each lattice design to meet the desired functionality. Physically, *I* delineate how much energy is lost to other parts of the system to cause damage during low strain compression. Using $\sigma_d = 80$ MPa and ε_d (specific for every lattice design) to define the upper limit stress and strain as proposed by Gruenbaum and Miltz[11], the RD-FRD achieved the highest *I*. Moreover, in terms of stiffness, the FRD lattice is superior irrespective of the design considerations. Its superior topological configuration played a major role in resisting axial deformation. Nevertheless, when graded on cell size, it consistently portrayed high mechanical performance.

Table 3 Summary of compressive cellular material properties.

Sample	$\mathbf{E_a}$[MPa]	$\boldsymbol{\sigma_Y}$[MPa]	$\boldsymbol{\sigma_U}$ [MPa]	$\boldsymbol{\varepsilon_d}$	**SEA** [MJ/kg]	I [%]
G	3,436.49	11.84	40.48	0.72	20.30	43.00
D	5,638.47	16.86	57.05	0.74	27.10	57.50
FRD	4,935.56	15.69	58.18	0.73	33.40	70.80
RD-G	3,146.87	11.09	47.57	0.74	25.80	54.90
RD-D	5,192.06	17.45	66.85	0.75	30.10	63.80
RD-FRD	4,285.91	13.82	77.71	0.75	41.30	87.60
CS-G	3,699.74	12.26	43.79	0.76	24.10	51.10
CS-D	5,456.06	16.89	61.17	-	-	-
CS-FRD	8,317.24	18.65	81.53	0.76	31.10	66.10
Multi-1 (G-D)	3,933.27	13.51	51.99	0.71	20.10	42.70
Multi-2 (FRD-G)	4,260.67	14.05	50.20	0.72	22.10	47.00
Multi-3 (FRD-D)	4,419.01	15.24	66.97	0.73	31.00	63.80
Multi-4 (FRD-D-G)	4,490.59	15.33	55.69	0.72	23.30	49.40
Multi-E1	5,634.64	15.97	56.00	0.73	29.40	62.30

4. CONCLUSION

The compressive properties of the G, D, and FRD lattices were studied numerically. The findings are summarised below;

- Functional grading of the lattice topology showed to considerably improve the compressive properties of the lattice core, on account of the change in failure behavior.
- Multi-segment cell layer failure is noticed with the FRD topology. This type of failure behavior is unique. Therefore, the uniform FRD lattice does not experience shear-band

failure, unlike other investigated uniform sheet-TPMS topologies. This failure mode is highly desirable for high-energy absorption. Hence, the reason why the FRD lattice exhibited the best compressive properties among the uniform property lattices.

- Consistent peaks and valleys in stress levels are noticed, which comes owing to densification and collapse of cell layers in that order. A similar trend is visualized with the hybrid topologies. However, a singled-out stress peak is observed when the transition region starts to deform plastically. Furthermore, higher stiffness and yield strength of the hybrid lattice are achievable by positioning the topology with a relatively higher surface-area-to-volume ratio near the loading surface.
- Overall, the RD-FRD lattice achieved the best compressive properties. Hence, are recommended for metamaterial designs for applications where axial forces dominate. Hence, functional grading and hybridization did considerably improve the compressive properties of the lattice cores.

Acknowledgment

The authors acknowledge the financial support provided by Khalifa University under Award No. RCII-2019-003.

REFERENCES

[1] Abou-Ali, A.M., Al-Ketan, O., Rowshan, R. and Al-Rub, R.A. Mechanical response of 3D printed bending-dominated ligament-based triply periodic cellular polymeric solids. *Journal of Materials Engineering and Performance*(2019), *28*(4), pp.2316-2326.

[2] Al-Ketan, O. and Abu Al-Rub, R.K.. Multifunctional mechanical metamaterials based on triply periodic minimal surface lattices. *Advanced Engineering Materials*(2019), *21*(10), p.1900524.

[3] Maskery, I., Aboulkhair, N.T., Aremu, A.O., Tuck, C.J., Ashcroft, I.A., Wildman, R.D. and Hague, R.J. A mechanical property evaluation of graded density Al-Si10-Mg lattice structures manufactured by selective laser melting. *Materials Science and Engineering: A*(2016), *670*, pp.264-274.

[4] Al-Ketan, O., Lee, D.W., Rowshan, R. and Al-Rub, R.K.A. Functionally graded and multi-morphology sheet TPMS lattices: Design, manufacturing, and mechanical properties. *Journal of the mechanical behavior of biomedical materials*(2020), *102*, p.103520.

[5] Koehnen, P., Haase, C., Bueltmann, J., Ziegler, S., Schleifenbaum, J.H. and Bleck, W.. Mechanical properties and deformation behavior of additively manufactured lattice structures of stainless steel. *Materials & Design*(2018), *145*, pp.205-217.

[6] Montazerian, H., Mohamed, M.G.A., Montazeri, M.M., Kheiri, S., Milani, A.S., Kim, K. and Hoorfar, M.. Permeability and mechanical properties of gradient porous PDMS scaffolds fabricated by 3D-printed sacrificial templates designed with minimal surfaces. *Acta biomaterials* (2019), *96*, pp.149-160.

[7] Afshar, M., Anaraki, A.P. and Montazerian, H.. Compressive characteristics of radially graded porosity scaffolds architectured with minimal surfaces. *Materials Science and Engineering: C*(2018), *92*, pp.254-267.

[8] Yoo, D.J. and Kim, K.H. An advanced multi-morphology porous scaffold design method using volumetric distance field and beta growth function. *International Journal of Precision Engineering and Manufacturing*(2015), 16(9), pp.2021-2032.

[9] Al-Ketan, O. and Abu Al-Rub, R.K., MSLattice: A free software for generating uniform and graded lattices based on triply periodic minimal surfaces. *Material Design & Processing Communications*(2020), p.e205.

[10] Kempen, K., Thijs, L., Van Humbeeck, J. and Kruth, J.P.. Mechanical properties of AlSi10Mg produced by selective laser melting. *Physics Procedia*(2012), 39, pp.439-446.

[11] Gruenbaum, G. and Miltz, J.. Static versus dynamic evaluation of cushioning properties of plastic foams. *Journal of Applied Polymer Science*(1983), *28*(1), pp.135-143.

[12] Barsoum, Z. and Barsoum, I. Residual stress effects on fatigue life of welded structures using LEFM. *Engineering failure analysis*(2009), *16*(1), pp.449-467.